Acta Pharmaceutica Sinica B 2023;13(9):3817−3833

Chinese Pharmaceutical Association
Institute of Materia Medica, Chinese Academy of Medical Sciences

Acta Pharmaceutica Sinica B

www.elsevier.com/locate/apsb
www.sciencedirect.com

ORIGINAL ARTICLE

LPS adsorption and inflammation alleviation by polymyxin B-modified liposomes for atherosclerosis treatment

Huiwen Liu[a,†], Honglan Wang[a,†], Qiyu Li[c], Yiwei Wang[a], Ying He[b], Xuejing Li[b], Chunyan Sun[a], Onder Ergonul[d], Füsun Can[d], Zhiqing Pang[b,*], Bo Zhang[a,*], Yu Hu[a,*]

[a]*Institute of Hematology, Union Hospital, Tongji Medical College, Huazhong University of Science & Technology, Wuhan 430022, China*
[b]*School of Pharmacy, Fudan University, Key Laboratory of Smart Drug Delivery, Ministry of Education, Shanghai 201203, China*
[c]*Department of Cardiology, Zhongshan Hospital, Fudan University, Shanghai Institute of Cardiovascular Diseases, Shanghai 200032, China*
[d]*Koç University Iş Bank Center for Infectious Diseases (KUISCID), Lnfectious Diseases and Clinical Microbiology Department, Koç University School of Medicine and American Hospital, Istanbul 34010, Turkey*

Received 16 April 2023; received in revised form 30 May 2023; accepted 1 June 2023

KEY WORDS

Lipopolysaccharide;
Atherosclerosis;
Polymyxin;
Liposomes;
Macrophages

Abstract Chronic inflammation is critical in the onset and progression of atherosclerosis (AS). The lipopolysaccharide (LPS) level in the circulation system is elevated in AS patients and animal models, which is correlated with the severity of AS. Inspired by the underlying mechanism that LPS could drive the polarization of macrophages toward the M1 phenotype, aggravate inflammation, and ultimately contribute to the exacerbation of AS, LPS in the circulation system was supposed to be the therapeutic target for AS treatment. In the present study, polymyxin (PMB) covalently conjugated to PEGylated liposomes (PLPs) were formulated to adsorb LPS through specific interactions between PMB and LPS. *In vitro*, the experiments demonstrated that PLPs could adsorb LPS, reduce the polarization of macrophages to M1 phenotype and inhibit the formation of foam cells. *In vivo*, the study revealed that PLPs treatment reduced the serum levels of LPS and pro-inflammatory cytokines, decreased the proportion

*Corresponding authors.
E-mail addresses: zqpang@fudan.edu.cn (Zhiqing Pang), zhangbo19871987@126.com (Bo Zhang), dr_huyu@126.com (Yu Hu).
[†]These authors made equal contributions to this work.
Peer review under the responsibility of Chinese Pharmaceutical Association and Institute of Materia Medica, Chinese Academy of Medical Sciences.

https://doi.org/10.1016/j.apsb.2023.06.005

of M1-type macrophages in AS plaque, stabilized AS plaque, and downsized the plaque burdens in arteries, which eventually attenuated the progression of AS. Our study highlighted LPS in the circulation system as the therapeutic target for AS and provided an alternative strategy for AS treatment.

1. Introduction

As one of the fundamental pathologic alterations in the majority of cardiovascular diseases, atherosclerosis (AS) is a complex, progressive, and multifaceted illness possessing properties of lipid deposition, inflammatory cell aggregation, and ultimate atheromatous plaques occurring in artery walls, which poses significant challenges to human health and generates an enormous economic burden[1,2]. Despite its unclear etiology, there is a growing consensus that systemic and chronic inflammation is closely linked to the onset and development of AS, which has been further supported by interventional studies showing that anti-inflammatory therapies, such as interleukin-1β antibody canakinumab, could attenuate the hazard of cardiovascular diseases[3]. In addition, except for traditional risk factors, including smoking, type 2 diabetes, obesity, and hypertension, emerging evidence has been accumulated to show that bacterial infection might play an essential role in the pathogenesis of AS[4−6], which might be the fountainhead of inflammation occurring in AS. It is believed that a profound definition of the inflammation mechanism underlying AS development could help identify novel therapeutic targets for preventing AS progression.

Lipopolysaccharide (LPS), a component of Gram-negative bacterial cell walls, can elicit a solid systematic inflammatory reaction once released into the blood[7]. A large amount of evidence from cross-sectional studies and prospective analyses has been accumulated to demonstrate that elevated circulating LPS level is closely associated with AS development and the clinical sequelae of AS progression, such as coronary heart disease, ischemic stroke, myocardial infarction, and cardiovascular death[6,8−13]. Moreover, results of human samples showed that the presence of LPS was only found in atherosclerotic arteries and not in normal ones. Furthermore, the level of LPS in the atherosclerotic plaque is positively aligned with that in the circulation system, and LPS passing through vascular endothelium can also induce vascular inflammation[14]. Regarding the mechanism, LPS stimulates vascular endothelial cells to produce adhesion molecules and recruits circulating blood monocytes to adhere to endothelial cells[2,15]. In addition, LPS and LPS binding protein (LPS−LBP) complexes can stimulate recruited monocytes through binding with CD14 and further activating toll-like receptor-4 (TLR4), which leads to skewing the balance toward M1-type differentiation, inducing the release of pro-inflammatory cytokines and exacerbating inflammation of blood vessels eventually[16]. Besides, macrophages with inflammatory polarization exhibit an attenuated ability for cholesterol transport and tend to become lipid-laden foam cells by engulfing oxidized low-density lipoprotein (ox-LDL)[17]. Furthermore, LPS-stimulated macrophages are inclined to migrate into the subintima and secrete matrix metalloproteinases, thus degrading the substrate, rupturing the atherosclerotic plaque, and leading to thrombogenesis threatening human life[18]. In summary, LPS and macrophages collectively contribute to AS development. It was believed that eradicating LPS and inhibiting macrophage polarization toward the M1 phenotype might be a promising strategy to alleviate AS effectively[1].

Different strategies have been developed for LPS clearance under different pathologic conditions. Antibodies specific to LPS, such as the HA-1A antibody, have been investigated in pediatric meningococcal septic shock. However, the results of clinical trials were far from satisfactory. Besides, antibodies were always of high price and relatively low stability[19,20]. In addition, macrophage-mimetic hybrid liposomes, which inherited the LPS binding sites from macrophage membranes, displayed a favorable LPS adsorbing ability and exhibited an excellent therapeutic effect for managing sepsis[21]. However, the method and the quality control for large-scale industrial production of macrophage membranes have yet to be well developed, which might limit the clinical transformation of macrophage-mimetic hybrid liposomes[22]. Small molecular compounds, such as polymyxin B (PMB), have been proposed as decent candidates for LPS adsorption. PMB was positively charged and could electrostatically adsorb anionic LPS[23]. In addition, the functional binding of PMB and LPS is stereospecific, and the high affinity of PMB with LPS is partly due to hydrophobic interaction as the driving force[24,25]. However, PMB is a small molecule drug, and the pharmacokinetics is always unfavorable. PMB could be easily bound to tissues, especially the muscle tissue, and the serum level of PMB decreased rapidly, which partially explained why the efficacy of PMB on removing circulating LPS in clinics was far from satisfactory[26]. Besides, PMB's severe nephrotoxicity and nerve block side effects also greatly restrict its utility in clinics[27]. Evidence has been accumulated in recent decades to demonstrate that the pharmacokinetics and *in vivo* tissue distribution of free drugs can permanently be altered to be more favorable when encapsulated into or modified on the surface of the liposome, resulting in reduced side effects and increased therapeutic benefits[28]. In addition, the modification of PEG to the liposome surface substantially weakens the liposome's rapid clearance by the mononuclear phagocyte system, thus harboring a long circulation half-life[29]. Therefore, PMB might function more efficiently and safely as a tool to adsorb LPS when formulated into PEGylated liposomes.

In this study, PMB was modified on the surface of PEGylated liposomes *via* covalent conjugation to form PLPs to remove circulating LPS for AS treatment (Fig. 1). The ability of PLPs to sponge LPS and its subsequent efficacy, such as prevention of macrophage activation, amelioration of inflammation response, restraint of foam cell formation, stabilization and reduction of AS plaque, and the potential therapeutic mechanism, were investigated both *in vitro* and *in vivo*. Our study highlighted that LPS removal was critical in AS therapy, providing an alternative strategy for AS treatment.

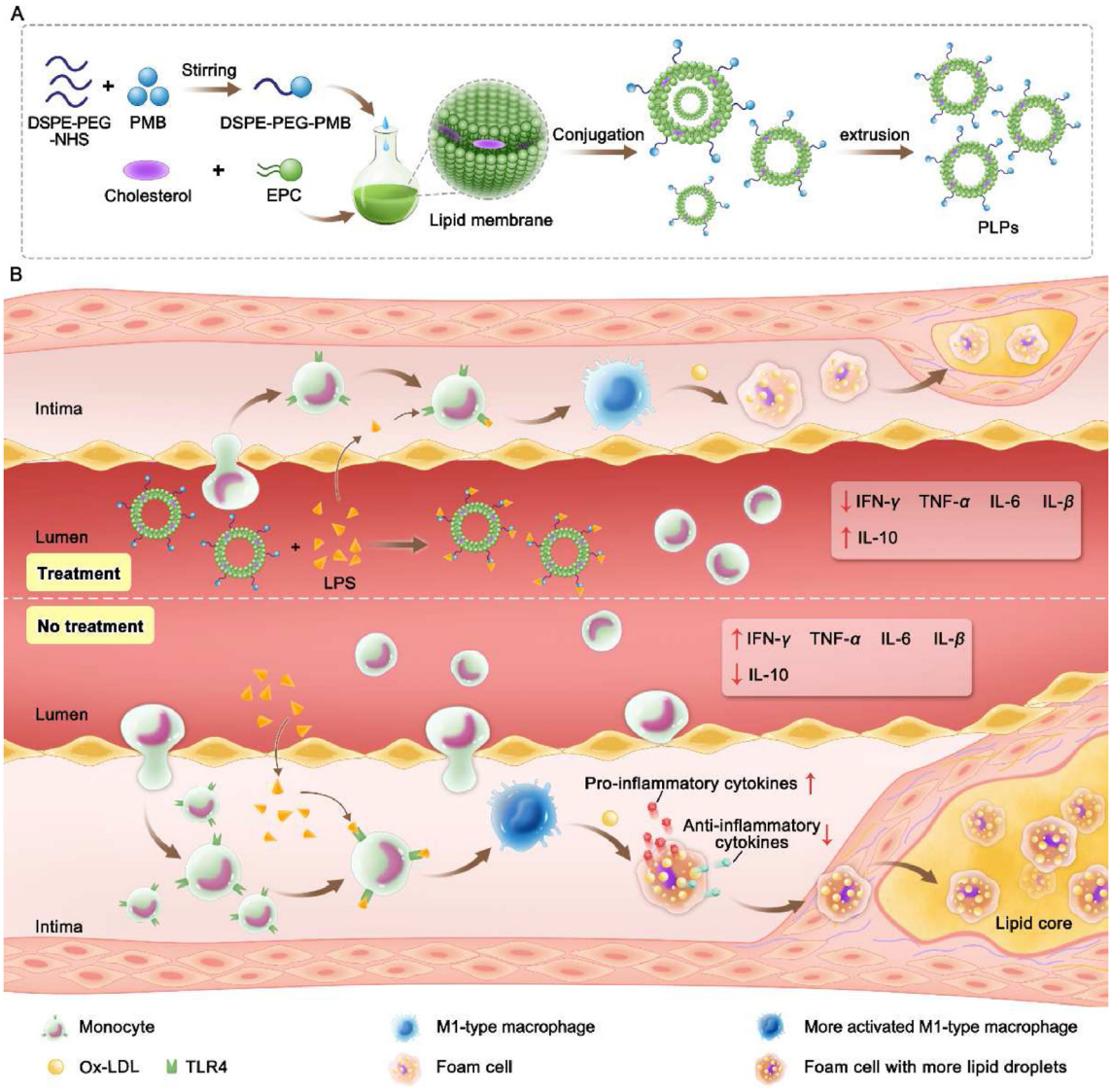

Figure 1 Schematic depiction of the preparation process of PLPs (A) and the mechanism underlying the therapeutic effect of PLPs on atherosclerosis (B). PLPs sponged LPS in the circulation system, decreased the amount of LPS passing through vascular endothelium into the intima, inhibited monocyte recruitment, macrophage polarization into M1-type, foam cell formation, and the secretion of pro-inflammatory cytokines, which is beneficial to the reduction of atherosclerotic plaque burden.

2. Materials and methods

2.1. Materials and animals

Anti-TLR4 antibody (FNab09837), Cy3-conjugated goat anti-mouse IgG (FNSA-0077), and PE-conjugated anti-mouse F4/80 antibody (FNab02922) was purchased from Wuhan Fine Biotech Co., Ltd. (Wuhan, China). The IL-1β-, IL-6-, and IL-10-ELISA kits were obtained from MultiSciences Biotechnology Co., Ltd. (Hangzhou, China). The IFN-γ- and TNF-α- ELISA kits were bought from Absin Biological Technology Co., Ltd. (Shanghai, China). The CCK8 kit was obtained from keyGEN Biotech Co., Ltd. (Jiangsu, China). Egg yolk lecithin (EPC) and 1,2-distearoyl-*sn*-glycerol-3-phosphoethanolamine-*N*-succinimidyl (polyethylene glycol)-2000 (DSPE-PEG2000-NHS) were acquired from AVT Pharmaceutical Tech Co., Ltd. (Shanghai, China). Cholesterol was obtained from Aladdin Company (Shanghai, China). Antibodies, including anti-CD80-PE (104707) and anti-F4/80-APC (157306), were obtained from Biolegend (San Diego, CA, USA). Dulbecco's modified Eagle medium (DMEM), fetal bovine serum (FBS), and penicillin−streptomycin were bought from Gibco (Carlsbad, CA, USA). Recombinant murine macrophage colony-stimulating factor (M-CSF) was from PeproTech (Cranbury, NJ, USA). FITC-conjugated Lipopolysaccharide (FITC-LPS) was from Sigma−Aldrich (St Louis, MO, USA). Oxidized low-density lipoprotein (ox-LDL) was from Yiyuan Biotechnology (Guangzhou, China). The oil red O staining kit was purchased from Beijing Solarbio Science & Technology Co., Ltd. (Beijing, China). polymyxin B was obtained from Sinopharm Chemical Reagent Co., Ltd. (Shanghai, China). The lipopolysaccharide testing kit was purchased from Shanghai Jianglai Biotechnology Co., Ltd. (Shanghai, China). The Lyso-Tracker Red and 4,6-diamino-2-

phenyl indole (DAPI) was purchased from Beyotime Biotechnology Co., Ltd. (Jiangsu, China). Anti *Escherichia coli* lipopolysaccharide (LPS) antibody (ab35654) was bought from Abcam (Cambridge, UK).

Six-week-old male mice lacking apolipoprotein E (*ApoE*$^{-/-}$) and C57/BL6J mice were purchased from Beijing Vital River Laboratory Animal Technology Co., Ltd. (Beijing, China) and Lingchang Biotech (Shanghai, China), respectively. All mice were housed in a specific pathogen-free experimental animal center at the School of Pharmacy, Fudan University. The Animal Ethics Committee, Fudan University provided ethics approval for the protocols involving animal experiments that were conducted conforming to national guidelines.

2.2. Cell culture

The murine RAW264.7 cell and HUVEC cell lines were from the Chinese Academy of Sciences Cell Bank (Shanghai, China). Both cells were grown in DMEM medium supplemented with 10% FBS and 1% penicillin−streptomycin and maintained in a humidified environment at 37 °C and 5% CO_2.

2.3. Fabrication and characterization of PLPs

PLPs were formulated utilizing a thin-film hydration process as previously described[30]. Firstly, 9 mg of phosphatidylcholine and 3 mg of cholesterol were dissolved in 10 mL of dichloromethane in a 50 mL round-bottom flask, which was subjected to vacuum evaporation to form a thin lipid film. Secondly, DSPE-PEG2000-PMB was synthesized as follows: 2.9 mg of DSPE-PEG2000-NHS in 100 μL of DMSO was mixed with 1.3 mg of PMB in 500 μL of double distilled water, followed by stirring at 400 rpm for 1 h at room temperature. Thirdly, 200 μL of DSPE-PEG2000-PMB from the second step and 1 mL of water were added to the flask in the first step to hydrate the thin layer at 37 °C. Finally, the mixture was sonicated for approximately 10 min at 4 °C with a sonicator and extruded through a 100 nm polycarbonate porous membrane using an extruder apparatus (Avestin, LF-1, Canada) for 20 times to obtain PLPs. The control liposomes (LPs) were formulated utilizing the same procedures as PLPs without PMB.

The structures and morphology of PLPs were observed using cryo-electron microscopy (Cryo-EM) (Tecnai G2 F20; FEI, Eindhoven, Netherlands) with liquid nitrogen. The size distribution and zeta potential of PLPs were measured by dynamic light scattering (ZEN3600 Zetasizer, Malvern, UK). In addition, the diameter and zeta potential of PLPs in deionized water were used as the indicators of stability, and both were monitored every day over seven days.

2.4. LPS adsorption studies

PLPs (0.4 mg) were mixed with various amounts of FITC-LPS (40, 80, 160, and 320 ng) in 0.4 mL of pathogen-free water or PBS. As a parallel experiment, the FITC-LPS amount was fixed at 320 ng in 0.4 mL of pathogen-free water or PBS, and different amounts of PLPs (0.5, 1, 2, and 3 mg/mL) were added. In both experiments, the liposomes were precipitated by ultracentrifugation at 100,000×*g* for 45 min (Hitachi, CP100NX, Tokyo, Japan) after incubation at 37 °C for 30 min. The unbound FITC-LPS in the supernatant was measured by a microplate reader at Ex/Em of 488/562 nm (BioTek, Synergy H1, Vermont, USA). The fluorescence intensities of FITC-LPS with different concentrations were plotted as a standard curve. Equal amounts of LPs and PMB were used as control groups.

2.5. Isolation and culture of BMDMs (bone marrow-derived macrophages)

BMDM isolation procedures were described as previously reported[31]. In brief, C57/BL6J mice were euthanized, and their femurs and tibias were excised. The marrow cavities were flushed with 1 mL of sterile PBS, and the fluid was filtered through a 45 μm nylon mesh to obtain bone marrow cells. Following erythrocyte lysis, the remaining cells were pelleted and cultured in DMEM complete medium containing 20 ng/mL of recombinant murine M-CSF at a cell density of 4×10^6/mL for seven days in total. On the last day, the medium was replaced with a complete medium without M-CSF for further use.

2.6. Inhibition of LPS-induced BMDM activation by PLPs in vitro

LPS (100 ng/mL) was mixed with equivalent amounts of PMB, LPs, or PLPs (0.5 mg/mL) in PBS and incubated at 37 °C for 30 min. The supernatant was collected after the mixture was ultracentrifuged at 100,000×*g* for 45 min. The BMDMs were isolated and cultured as methods in section 2.5 described. After seven days of culture, BMDMs were randomly divided into five groups, including PBS, LPS, PMB, LPs, and PLPs groups. BMDMs were incubated with PBS, LPS (100 ng/mL), or the supernatant mentioned above for 24 h, respectively. Then the induced macrophages were scraped off the Petri dish and washed twice with PBS. The proportion of M1-type macrophages remarked by F4/80 and CD80 double-positive was analyzed by flow cytometry (Beckman Coulter Inc., Brea, CA, USA). Besides, the cell supernatant in each group was collected after centrifugation at 1200 rpm for 5 min (Thermo Fisher, Tx-400, Waltham, MA, USA) and then subjected to an ELISA test to quantify the concentrations of different types of inflammatory cytokines such as TNF-α, IL-1β, IL-6, IFN-γ, and IL-10 following the manufacturer's instructions.

2.7. Foam cell formation assay and RNA sequencing

The BMDMs at a density of 5×10^5 cells per well in six-well plates were cultured in DMEM complete medium, which was added with ox-LDL (50 μg/mL) plus PBS, LPS (100 ng/mL) or the three types of supernatants obtained as described in method section 2.6. After incubation for 24 h at 37 °C, cells were immobilized with 10% formalin, rinsed in 60% isopropanol, stained with modified oil red O (ORO) stain solution, and counterstained with Mayer's hematoxylin solution. Images were captured utilizing an inverted microscope (Olympus, CKX53, Tokyo, Japan). Cells possessing one or more ORO-positive lipid droplets were defined as foam cells[32], and the proportion of foam cells in each group was calculated by ImageJ software.

Except for oil red O staining, BMDMs subjected to the same treatment were also used for RNA sequencing. Following two washes with PBS, 500 μL of TRIzol was added to each well of a 6-well plate to extract RNA, and high-quality RNA samples were chosen by an RNA 6000 Nano LabChip Kit (Agilent 5067−1511, Santa Clara, CA, USA) to construct a sequencing library. Following purification using Dynabeads Oligo (dT) (Thermo Fisher, Waltham, MA, USA), mRNA was fragmented into short

fragments and reverse-transcribed to creat cDNA by SuperScript™ II Reverse Transcriptase (Invitrogen, cat. 1896649, USA), which were then used to synthesize U-labeled second-stranded DNAs. After ligation with dual-index adapters, the products were amplified with PCR. Finally, 2 × 150 bp paired-end sequencing (PE150) of each sample was pooled and sequenced on an Illumina Novaseq™ 6000 (LC-Bio Technology Co., Ltd., Hangzhou, China). The differentially expressed genes (DEGs), identified with the parameter of false discovery rate (FDR) below 0.05 and absolute fold change ≥2, were then subjected to enrichment analysis of the Kyoto Encyclopedia of Genes and Genomes (KEGG) pathways. The histogram, KEGG enrichment scatter plots, and Advanced Heatmap Plots were generated using the OmicStudio tools at https://www.omicstudio.cn.

2.8. Cell uptake assay

DiD-labeled LPs and PLPs were fabricated by the same method described in method 2.3, except that 24 μg of DiD (0.2%, *w*/*w*) was added into dichloromethane solution containing 9 mg of phosphatidylcholine and 3 mg of cholesterol in advance. BMDMs were seeded into confocal petri dishes at a density of 4×10^5 cells per dish and cultured for 12 h. After that, 1 mL of DMEM containing 200 ng of FITC-LPS plus 800 μg of DiD-PLPs or not was added and incubated for 10 min, 2, and 4 h, respectively. Subsequently, the medium was removed, and cells were rinsed with PBS, fixed in 10% formalin, blocked with 1% BSA in PBS, and stained with anti-TLR4 antibody (1/200, *v*/*v*), Cy3-labeled secondary antibody, and DAPI successively. Fluorescence images were captured using a laser scanning confocal microscope (CLSM, Carl Zeiss, LSM710, Oberkohen, Germany).

2.9. Pharmacodynamic study of PLPs in vivo

ApoE$^{-/-}$ mice aged six weeks were fed *ad libitum* with a Western Diet (D12109C, Research Diet, New Brunswick, USA) for sixteen weeks to establish AS mouse models. Then mice were randomly assigned to different treatment groups, including PBS, LPs, and PLPs groups, in which mice received 100 μL of intravenous injections of PBS, LPs, or PLPs at a liposome dose of 0.5 mg every three days over sixteen weeks. At the termination of the study, the mice were weighed, euthanized, and subjected to heart perfusion with 20 mL of PBS. The aortas were removed from the proximal ascending segment to the branches of the iliac artery free of periadventitial fat. The lipid accumulation of the artery tree was determined by en-face oil red O (ORO) staining, and the percentage of lipid lesion area to the total aortic area was calculated by ImageJ software.

The aortic roots were embedded in OCT, frozen quickly, and cross-sectioned serially (8 μm thickness) starting from where the two aortic valves first appeared for histological analyses. The sections were subjected to ORO staining for lipid lesion observation, H&E staining for evaluation of necrotic cores in plaques, Masson's trichrome staining for collagen content assessment, α-SMA immunohistochemical staining for fibroblast content assessment[33], CD80 immunofluorescence staining for M1-type macrophage observation, and LPS immunofluorescence staining for evaluation of the amount of LPS. Four randomly selected slices per indicator were evaluated in each group. Then, the section images were acquired using a slice scanner (VS200, Olympus, Tokyo, Japan) and analyzed by ImageJ software.

To measure the serum level of LPS and inflammatory cytokines, including IFN-γ, TNF-α, IL-1β, IL-6, and IL-10, 50 μL of serum from *ApoE*$^{-/-}$ mice were collected in the 1st week, 8th week, and 16th week during the western diet feeding period. The serum concentration of LPS was measured using commercial ELISA kits according to the manufacturer's procedures. The serum level of five different inflammatory cytokines in mice was analyzed utilizing a Mouse Magnetic Luminex Assay (LXSAMSM-05, R&D Systems, Minneapolis, MN, USA).

2.10. Biocompatibility study of PLPs

HUVECs were seeded into 96-well plates at a density of 3×10^3 cells per well. A culture medium containing different amounts of PLPs was added to cells (100 μL per well), and equivalent amounts of free PMB and blank liposomes were used as controls. After being incubated for 24 h, cells were subjected to 10 μL of CCK8 solution for another 1.5 h. The absorbance at 450 nm was measured with a microplate reader (BioTek). The cell viability was normalized to the PBS treatment group. In addition, at the termination of the pharmacodynamics study, the AS mouse models were subjected to retro-orbital puncture to collect blood for routine blood tests and biochemical analysis. Major organs, including the heart, liver, spleen, lung, and kidney, were also collected, weighed, and sectioned for H&E staining.

2.11. Pharmacokinetics and distribution of PLPs arresting LPS in vivo

For the LPS−PLPs group, 100 ng of FITC-LPS was pre-incubated with 600 μg of DiD-labeled PLPs at 37 °C for 30 min and then intravenously injected into C57/BL6J mice. For the LPS + PLPs group, an equal amount of FITC-LPS and DiD-labeled PLPs were mixed and intravenously injected into C57/BL6J mice immediately. Mice receiving DiD-labeled PLPs alone served as a control group. 30 μL of blood was collected by a postorbital puncture at different time points (1 or 15 min, 1, 2, 4, 8, 12, and 24 h post-injection) and mixed with 70 μL of PBS for fluorescence measurement in a 96-well plate at Ex/Em of 640/670 nm. The pharmacokinetics curve was plotted, and the circulation half-time was calculated by DAS 2.0 software.

To examine the distribution of PLPs arresting LPS *in vivo*, 12 h after injection, mice were euthanized, then spleens and livers were isolated, frozen, and sectioned. After being stained with DAPI and PE-anti-F4/80 antibodies, the slices were observed under a CLSM (Carl Zeiss) to evaluate the colocalization of LPS and PLPs or LPS−PLPs complexes and macrophages. For the distribution study, 24 h post-injection, mice were euthanized and perfused with 30 mL of PBS. Then, major organs were collected, weighed, and homogenized with PBS (1:3, *w*/*w*) in an ice bath by a tissue homogenizer (YPH-Bio, Bioprep-24, Beijing, China). The fluorescence intensity at Ex/Em of 640/670 nm was measured.

2.12. Statistical analysis

The results were analyzed using GraphPad Prism 8. An unpaired Student's *t*-test or one-way ANOVA was used to evaluate significant differences between two groups or among multiple groups.

The results are presented as the mean ± standard error of the mean (SEM). A P value of <0.05 was considered a statistically significant difference.

3. Results and discussion

3.1. Characterization of PLPs

LPs and PLPs were hollow spheres with smooth surfaces and dispersed as single particles under Cryo-TEM (Fig. 2A). The diameters of LPs and PLPs were 151.50 ± 2.11 and 164.30 ± 3.60 nm, respectively (Fig. 2B), and their zeta potentials were −19.87 ± 0.26 and 1.94 ± 0.08 mV, respectively (Fig. 2C). The slight increase in diameter and inverse change in zeta potential was probably due to the surface modification of cationic PMB on liposomes through an amide condensation reaction. When suspended in the sterile water at 4 °C, PLPs remained stable with a mean size of 150 nm and an average Zeta potential of 2.0 mV during one-week storage (Fig. 2D and E), which indicated favourable stability of PLPs. These physio-chemical characterizations of PLPs conformed well to the requirements for *in vivo* study as previously reported[34,35]. It was estimated that the encapsulation efficacy of PMB in liposomes was 17.30 ± 0.45%, and the drug loading capacity was 1.49 ± 0.04%.

3.2. LPS adsorption by PLPs in vitro

Two sets of parallel experiments were carried out to investigate the ability of PLPs to sponge LPS. Firstly, a fixed concentration of PLPs (1 mg/mL) was incubated with different amounts of LPS (40, 80, 160, and 320 ng). After incubation and ultracentrifugation, the concentration of remaining LPS in the supernatant was quantified (Fig. 2F and G, Supporting Information Fig. S1 A and S1B). Besides, the LPS adsorption capacity of PLPs was also quantified by incubating fixed LPS (800 ng/mL) with various amounts of PLPs (0.2, 0.4, 0.8 and 1.2 mg) (Fig. 2H and I, Supporting Information Fig. S1 C and S1D). As the results showed, the proportion of LPS sponged was inversely correlated with the amounts of LPS added and proportional to the amounts of PLPs added in water, which was in line with the trend in PBS. It was estimated that approximately 1 mg of PLPs could sponge 175 ng of LPS, while 1 mg of LPs could only sponge 50 ng of LPS. The

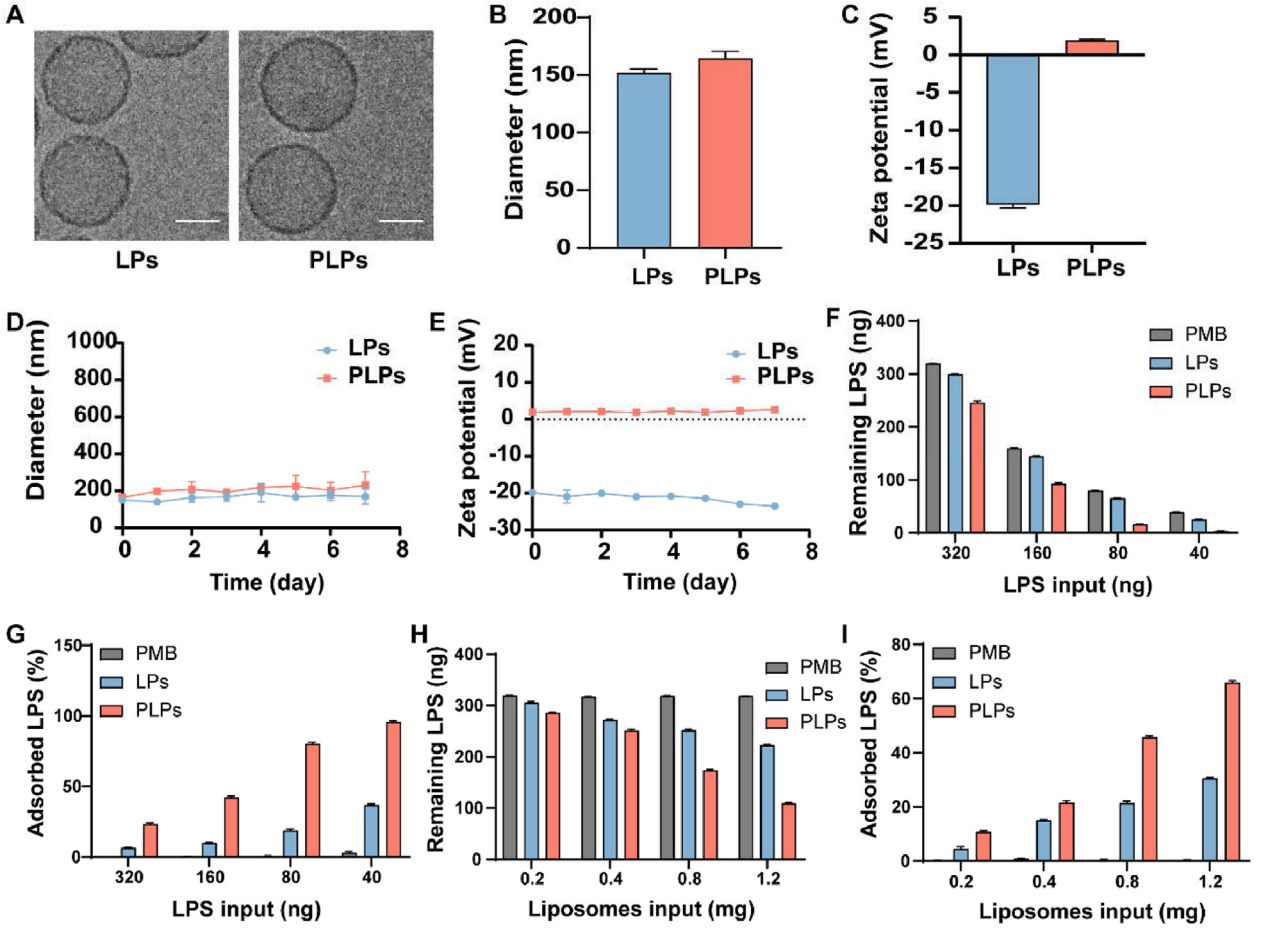

Figure 2 Characterization of PLPs. (A) Representative Cryo-TEM images of LPs and PLPs. Scale bar = 100 nm. (B) Particle size and (C) surface zeta potential of LPs and PLPs analyzed by dynamic light scattering. (D, E) The stability of LPs and PLPs was indicated by particle size (D) and zeta potential (E) when stored in deionized water at 4 °C for one week. (F) The remaining LPS and (G) the adsorbed LPS after a fixed amount of PLPs (1 mg/mL) were incubated with LPS of various amounts in water. (H) The remaining LPS and (I) the adsorbed LPS after a fixed amount of LPS (800 ng/mL) were incubated with PLPs of various amounts in water. LPs and PMB served as control groups. All experiments were repeated three times, and the data were presented as the mean ± SEM (n = 3).

results above confirmed that PLPs exhibited superb LPS adsorption ability compared with LPs in water and a simulated *in vivo* environment, probably through electrostatic and hydrophobic interactions between PMB modified on the surface of PLPs and LPS.

The influence of the protein corona on the binding of PLPs and LPS was also investigated. The PLPs of different amounts were pre-incubated with serum at 37 °C for 1 h before incubation with LPS. The results (Supporting Information Fig. S2) demonstrated that the protein corona did not strongly affect the adsorption ability of PLPs on LPS, and increasing the dose of PLPs could elevate the adsorption effect of PLPs on LPS to achieve the desired adsorption effect.

The binding capacity of PLPs with LPS was also evaluated. First, the PLPs were incubated with FITC-LPS in water or mice serum for a series of time points, after which they were ultracentrifuged. Second, the pellet at the time point of 0.5 h was resuspended in 0.4 mL of mouse serum, and the solution was stirred and ultracentrifuged again. Results illustrated that LPS was adsorbed in more significant quantities as the incubation period prolonged and reached a peak proportion at 60 h. The adsorption rate of LPS was 83.12 ± 0.12% in water (Supporting Information Fig. S3 A) and 73.32 ± 1.54% in mouse serum (Supporting Information Fig. S3 B), respectively, and maintained the plateau till at least 72 h. The release rates of adsorbed LPS from the LPS−PLPs complex increased slowly as the stirring time prolonged, from 0.17 ± 0.03% at 0.5 h to a peak of 23.35 ± 2.59% at 48 h (Supporting Information Fig. S3 C). These results demonstrated that the departure of LPS from LPS−PLPs complexes was limited, and the release rate was significantly less than the binding efficiency of LPS with PLPs, suggesting that LPS could bind strongly to PLPs.

Previous papers reported that LPS-enhanced areas (LPS patches) across bacterial cell surface is where LPS is inserted into bacterial outer membranes[36,37]. Moreover, studies on the reconstruction of the outer membrane of *E. coli* have demonstrated that

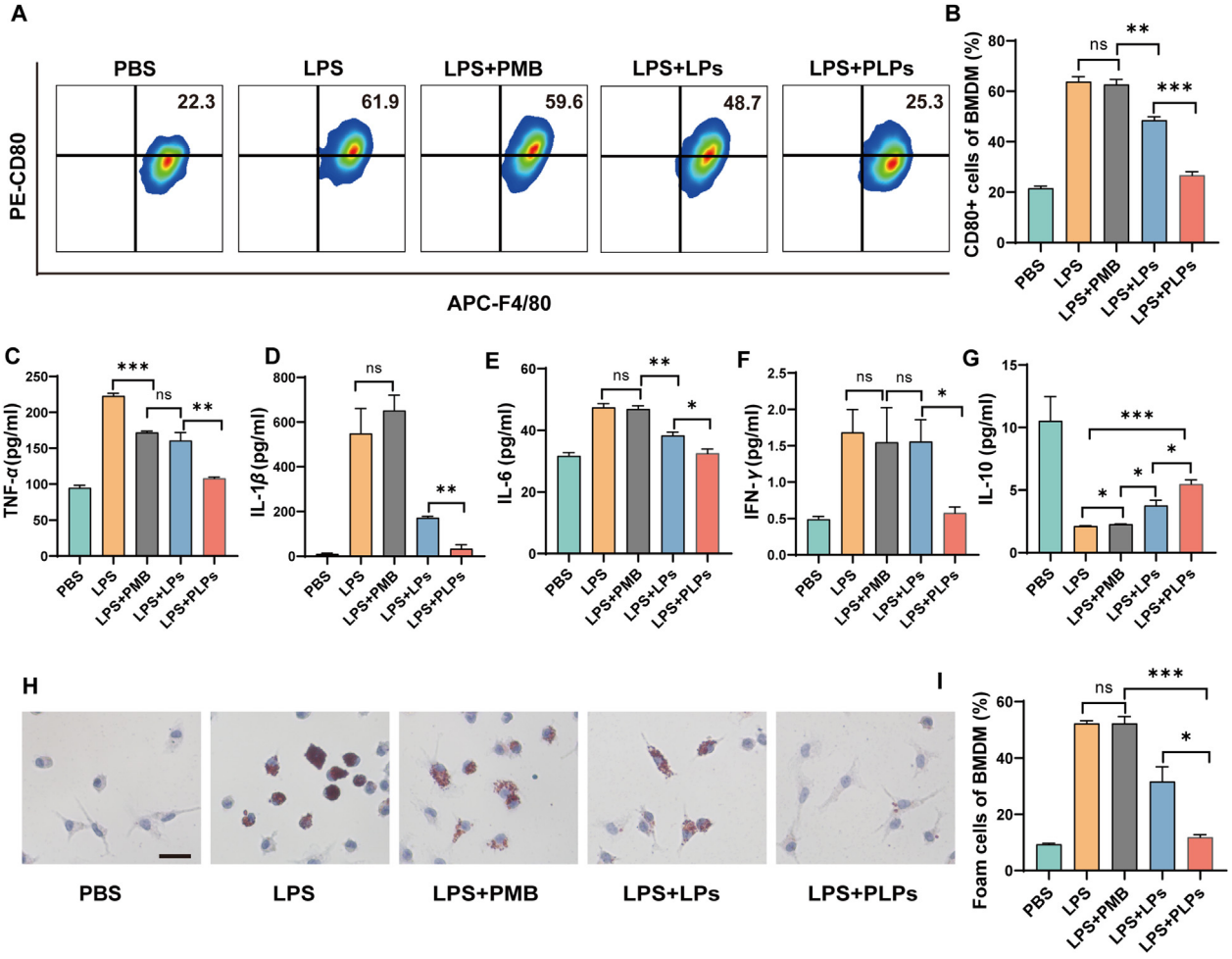

Figure 3 Inhibitive effect of PLPs on LPS-induced biologic behaviors of BMDMs. (A) Representative flow cytometry plots and (B) the corresponding quantification analysis of M1-phenotype macrophages treated with LPS alone or pre-incubated with PMB, LPs, or PLPs. The PBS-treated group was included as a control. (C−G) Expression levels of inflammatory cytokines, including TNF-α (C), IL-1β (D), IL-6 (E), IFN-γ (F), and IL-10 (G) in the supernatant of cell culture medium after different treatments. (H, I) The formation of foam cells induced by different treatments was analyzed qualitatively by an optical microscope (H) and quantitatively by ImageJ software (I), respectively. BMDMs with different treatments in the presence of ox-LDL (50 μg/mL) were subjected to ORO staining, and those positive staining cells were indicated as foam cells. Scale bar = 20 μm. The experiments were conducted three times independently. All data were presented as the mean ± SEM ($n = 4$). *$P < 0.05$, **$P < 0.01$, and ***$P < 0.001$. ns, not significant.

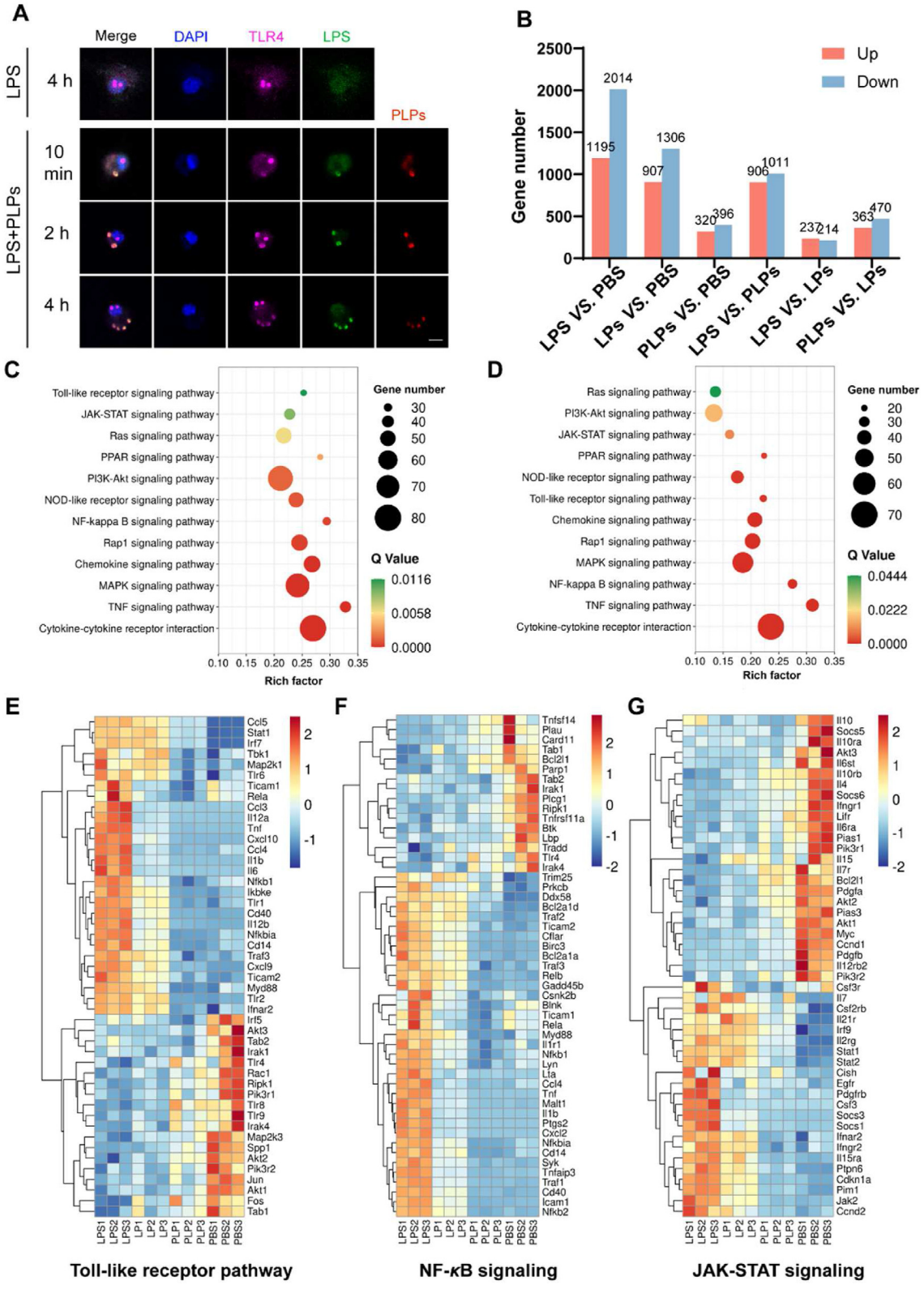

Figure 4 The mechanism underlying the inhibitive effect of PLPs on LPS-induced macrophage activation. (A) Fluorescence images of macrophages treated with LPS alone or mixed with PLPs over time. The cells were stained with anti-TLR4 antibodies on the surface and counterstained with DAPI for the nucleus. Scale bar = 10 μm. Green: FITC-labeled LPS. Red: DiD-labeled PLPs. Purple: Cy3-labeled anti-TLR4 antibodies. Blue: DAPI-stained nucleus. (B) The number of differentially expressed genes (DEGs) in macrophages between different treatment groups. (C) KEGG enrichment analysis illustrating significantly enriched signaling pathways in LPS *versus* PBS groups based on DEGs.

LPS could be incorporated into liposomes through extrusion−external mechanical force *in vitro*[38]. In this study, the binding between PMB modified on the liposome surface and LPS is stereospecific, with electrostatic and hydrophobic interactions as driving forces. Therefore, we speculate that LPS binding to the PMB increases the likelihood of interactions between LPS and liposomes, guiding and facilitating the insertion of LPS into the liposome membrane. The results (Fig. 2F−I and Supporting Information Fig. S1) showed that the adsorption efficiency of PLPs on LPS was significantly higher than that of LPs, which supported the hypothesis above to some extent.

3.3. Inhibitive effect of PLPs on LPS-induced macrophage activation

The effect of LPS sponged by PLPs *in vitro* was investigated using BMDMs as the macrophage model. As the results showed (Fig. 3A and B), the proportion of M1-type macrophages was 63.85 ± 4.02% and 62.60 ± 4.25% in the LPS group and PMB group, respectively, whereas the ratio in the PLPs group was sharply reduced to 26.70 ± 2.74%, which was close to the baseline in the PBS group (21.53 ± 0.89%), indicating PLPs could effectively block LPS-mediated macrophage activation by sponging LPS. In addition, it was revealed that LPS treatment could induce macrophages to secrete more pro-inflammatory cytokines (TNF-α, IL-1β, IL-6, and IFN-γ) compared with the PBS group, which was consistent with previous reports[39,40]. On the contrary, the level of pro-inflammatory cytokines was remarkably reduced, and IL-10 secretion was significantly elevated in the PLPs group, indicating the pro-inflammatory effect of LPS could be successfully reversed by PLPs treatment (Fig. 3C−G). Furthermore, utilizing oil red O staining for neutral lipids, it was found that PLPs decreased the proportion of foam cells substantially down to 11.85 ± 0.92%, in contrast to 52.24 ± 0.96% in the LPS group (Fig. 3H and I). This was probably attributed to LPS stimulation promoting Myd88-IRF1 interaction and IRF1 nuclear translocation in macrophages. Thus, macrophages enhanced ox-LDL uptake *via* scavenger receptors and eventually contributed to cholesteryl ester accumulation in the cytoplasm and the formation of foam cells[41], which could be successfully blocked by PLPs treatment *via* LPS sponging. Altogether, these results further confirmed that PLPs possessed a superb capacity for LPS adsorption, which was conducive to mitigating macrophage activation, diminishing pro-inflammatory cytokines release, and inhibiting foam cell formation. These results implied that PLPs probably had great potential for AS treatment *in vivo*.

3.4. The inhibitory mechanism of PLPs on LPS-induced macrophage activation

It was previously reported that LPS released from bacteria was firstly bound to LPS-binding protein (LBP) in the serum. Then the formed complex (LPS−LBP) dimerized TLR4 *via* CD14, initiated signaling transduction, and ultimately mediated the expression of excessive potent inflammatory mediators by macrophages[42]. Hence, dynamic observation of the interaction process of LPS, TLR4, and PLPs is favorable for exploring the mechanism underlying the inhibitive effect of PLPs on macrophage activation induced by LPS. As shown in Fig. 4A, free LPS substantially bound to TLR4 on the surface of macrophages at 10 min after incubation, and it was noted that LPS and PLPs could be highly and rapidly colocalized upon PLPs addition, which demonstrated the strong ability of PLPs to seize LPS securely and the high-affinity PLPs−LPS complex formation. It was also revealed that macrophages internalized the LPS−PLPs complex as a whole in a time-dependent manner (Fig. 4A). According to the results above and a previous study[30], it was speculated that LPS adsorbed by PLPs was no longer available to TLR4 on the surface of macrophages, and the downstream pro-inflammatory signaling pathway of TLR4 could not be activated.

In order to verify the hypothesis above, RNA sequencing was also applied to explain the underlying molecular mechanism of the impact of PLPs on LPS-induced macrophage activation. After being treated with PBS, LPS, LPS plus LPs, or LPS plus PLPs for 24 h, BMDMs were collected for RNA-Seq analysis. The number of differentially expressed genes (DEGs) in different groups is shown in Fig. 4B. A total of 3209 genes were differentially expressed between the LPS and PBS groups, of which 1195 genes were upregulated, and 2014 genes were downregulated in LPS-stimulated macrophages versus PBS-treated macrophages. The number of DEGs from LPS *vs.* PBS, LPs *vs.* PBS, and PLPs *vs.* PBS groups were 3209, 2213, and 716, respectively, which could be explained by the gradually decreased LPS concentration and alleviated macrophage activation status. The KEGG enrichment scatter plot showed that a large number of signaling pathways known to promote inflammatory responses were significantly enriched in the LPS group in comparison with the PBS group, such as Toll-like receptor signaling pathway, NF-κB signaling pathway, JAK-STAT signaling pathway, and PI3K-Akt signaling pathway (Fig. 4C). Similar results were also observed in the LPS group compared with the PLPs group but not the LPs group (Fig. 4D). These results altogether validated that the addition of PLPs ablated the effect of LPS on the activation of macrophage inflammatory signaling pathways. Specifically, it was noticed that the PPAR signaling pathway, which is strongly related to cholesterol efflux during foam cell formation, was differentially expressed not only in the LPS *vs.* PBS but also in the LPS *vs.* PLPs groups but not in LPS *vs.* LPs group[43]. This finding aligned with the result that macrophages in the PBS and PLPs groups harbored less lipid accumulation than those in the LPS group (Fig. 3H), implying that the effect of LPS on the lipid metabolism of macrophages could be successfully reversed by PLPs treatment. The expression level of genes associated with the activation signaling pathway within the macrophage transcriptome was further assessed. As shown in Fig. 4E, the genes related to the Toll-like receptor pathway in the LPS group and LPs group were primarily clustered in the positive direction. However, the PLPs and PBS groups were concentrated mainly in the adverse order. Previous studies also demonstrated that NF-κB signaling and the JAK-STAT pathway exerted essential influences on macrophage polarization as canonical signaling pathways[44−46]. The results consistently showed a significant upregulation of related gene expression implicated in macrophage activation in the LPS and LPs groups, such as *Myd88*, *Cd14*, *Stat1*, and *Jak2*. However, an

(D) Based on DEGs, KEGG enrichment analysis illustrates significantly enriched signaling pathways in LPS *versus* PLPs groups. (E−G) Heatmap of hierarchical cluster analysis displaying normalized gene expression related to Toll-like receptor signaling, NF-κB signaling, and JAK-STAT signaling by different treatments.

opposite trend was found in the PLPs and PBS groups (Fig. 4F and G). Altogether, these results demonstrated that PLPs, in comparison with LPs, could arrest LPS and inhibit macrophage polarization toward the M1 phenotype by downregulating pro-inflammatory signaling pathways and reducing the expression of inflammatory genes.

3.5. *Pharmacodynamics experiment of PLPs on AS in vivo*

The therapeutic efficacy of PLPs on AS *in vivo* was evaluated on apolipoprotein E-deficient ($ApoE^{-/-}$) mice[47]. As shown in Fig. 5A and B, the red region stained with oil red O could reflect the plaque area of lipid deposition. The proportion of atherosclerotic lesions in the en face aorta of the PLPs group (39.9 ± 1.5%) was significantly less than that of the PBS group (73.6 ± 5.4%) and the LPs group (51.9 ± 2.0%). Consistent with the results in en-face aortas, the PLPs group harbored a significantly lower lipid accumulation ratio (31.2 ± 1.7%) in the plaque area, in contrast to that of the PBS group (52.3 ± 1.2%) and the LPs group (49.4 ± 0.8%) (Fig. 5C and G). These results demonstrated that PLPs reduced the atheroma burdens of AS model mice compared to the LPs and PBS groups. As shown by Supporting Information Fig. S4, the lowest proportion of necrotic cores in plaque areas characterized by acellular cores and cholesterol clefts was 17.32 ± 0.42% in the PLPs group, as compared with 38.46 ± 0.39% or 29.80 ± 1.14% in the PBS or LPs group, which demonstrated PLPs could effectively inhibit the progression of AS[48]. It was well documented that the collagen concentration around the AS plaque could reflect the fibrous cap thickness and α-SMA content in aortic plaques was positively correlated with the accumulation of vascular smooth muscle cells (VSMCs), which was involved in hindering atherosclerosis progression[49,50]. Therefore, both collagen and α-SMA were beneficial to stabilizing aortic plaques and could help prevent atherosclerotic plaque from rupturing to cause acute coronary syndrome and stroke[51,52]. Hence, in order to further evaluate the stability of plaques, collagen staining, and α-SMA staining were performed within cross-sectional lesions. As compared to PBS treatment (37.0 ± 1.2%), LPs and PLPs treatments elevated the collagen content ratio in plaque areas up to 45.7 ± 0.9% and 58.9 ± 3.0%, respectively (Fig. 5D and G). As shown in Fig. 5E and G, an increase of 11.84% and 4.18% of α-SMA content could be discerned in the PLPs group compared with the PBS and LPs groups, respectively. Therefore, PLPs treatment is beneficial in enhancing the stability of AS plaques in contrast to LPs and PBS treatments. Moreover, there is a positive correlation between the blood LPS concentration and the amount of LPS in atheromatous plaques[14]. The latter can trigger vascular inflammation, so we tested whether PLPs could also reduce the amount of LPS in plaques. As shown by Supporting Information Fig. S5, the lowest proportion of LPS area in tissues was found to be 2.43 ± 0.18% in the PLPs group, compared with 19.78 ± 1.98% and 12.01 ± 0.89% in the PBS and LPs groups, respectively. Plaque macrophages, the critical cells accounting for most immune cells in atherosclerotic plaques, represented the inflammatory status in AS plaques[15,53]. The pro-inflammatory M1 phenotype macrophages were highly involved in the progression of AS. Therefore, to estimate the quantity of M1 phenotype macrophages, we performed CD80 immunofluorescent staining on sections. The hemi-quantitative analysis revealed that the proportion of CD80 positive-M1 phenotype macrophages in total cells was decreased by 12.6% and 27.6% after LPs and PLPs treatments compared with PBS treatment (69.27 ± 2.88%) (Fig. 5F and G), demonstrating PLPs could effectively reduce the ratio of M1 macrophages and inhibit the inflammation status in AS plaques. Except for macrophages, endothelial and neutrophils were also reported to be involved in LPS-induced AS progression[54,55]. The inhibitive effect of PLPs on AS might also work through endothelial and neutrophils etc., which deserves further study to comprehensively understand the therapeutic effect of PLPs on AS.

Systematic chronic inflammation has been documented to exacerbate AS development, perhaps mediated by inflammatory macrophages through secreting pro-inflammatory cytokines into the circulation in response to tissue-derived signals, toxic molecules, and so on[1,17]. Thereby, the effect of PLPs on systematic inflammation in AS model mice was further explored. On the 1st, 8th, and 16th week, the serum from AS model mice was collected and subjected to ELISA kits for LPS quantification. As shown in Fig. 6A, compared to the cumulative LPS level in the PBS group, the LPS concentrations were always maintained at significantly low levels in the PLPs group, demonstrating that PLPs could effectively clear LPS *in vivo*. It was believed that the elevated LPS concentration in the circulation system contributed to polarizing macrophages to the M1 phenotype, which could produce more pro-inflammatory cytokines[56]. Taking TNF-α, a dominant cytokine in the AS development, as an example, the PBS group and LPs group displayed a continuous escalation of serum TNF-α level from 4.50 ± 0.25 to 6.31 ± 0.36 pg/mL and from 3.60 ± 0.18 to 4.90 ± 0.52 pg/mL, respectively. However, PLPs treatment resulted in a gradual decrease of TNF-α from 2.47 ± 0.32 to 1.71 ± 0.11 pg/mL, which was opposite to the trend observed in the PBS and LPs groups (Fig. 6B). Other inflammatory cytokines such as IL-1β, IL-6, and IFN-γ, also displayed a gradually upregulated expression in the PBS and LPs groups. In contrast, these increases were blocked by PLPs treatment to various degrees (Fig. 6C−E). Opposed to the kinetics of pro-inflammatory cytokines, IL-10, the anti-inflammatory cytokine, exhibited a slight declining trend in the PBS and LPs groups but a continuous increase in the PLPs group (Fig. 6F). The reduction of LPS in the blood conferred by PLPs corresponded to the decrease of pro-inflammatory cytokines in the circulation. This further demonstrated that PLPs could eradicate LPS effectively and inhibit the activation of macrophages and the inflammation responses in AS.

The inflammatory macrophages arising from exposure to LPS and other stimuli are characterized by a lipid metabolism disorder and therefore are more likely to form lipid-laden macrophages[57]. The latter, also denoted as foam cells, harbor lipid drops consisting of triacylglycerols (TGs) and cholesterol esters (CEs). TG synthesis is vital for pro-inflammatory macrophage function, inhibition of which decreases pro-inflammatory IL-1β and IL-6 as well as phagocytic capacity[58]. Meanwhile, inflammatory macrophages are inclined to change the expression of some scavenger receptors and decrease cholesterol efflux transporters, reducing their ability to lipid handling in the plaque, which accelerates AS progression[59]. Analysis of serum lipid profiles showed that PLPs treatment caused a significant decrease in total cholesterol (TC). At the same time, almost no effect was found on the levels of other lipid metabolism indicators, such as triglycerides (TG), HDL, and LDL (Fig. 6G−J)). It was proposed that LPS reduced cholesterol efflux transporter SR-B1 expression on macrophages, exerting a detrimental impact on cholesterol homeostasis[17,60,61]. Interestingly, PLPs partially improved cholesterol homeostasis, which

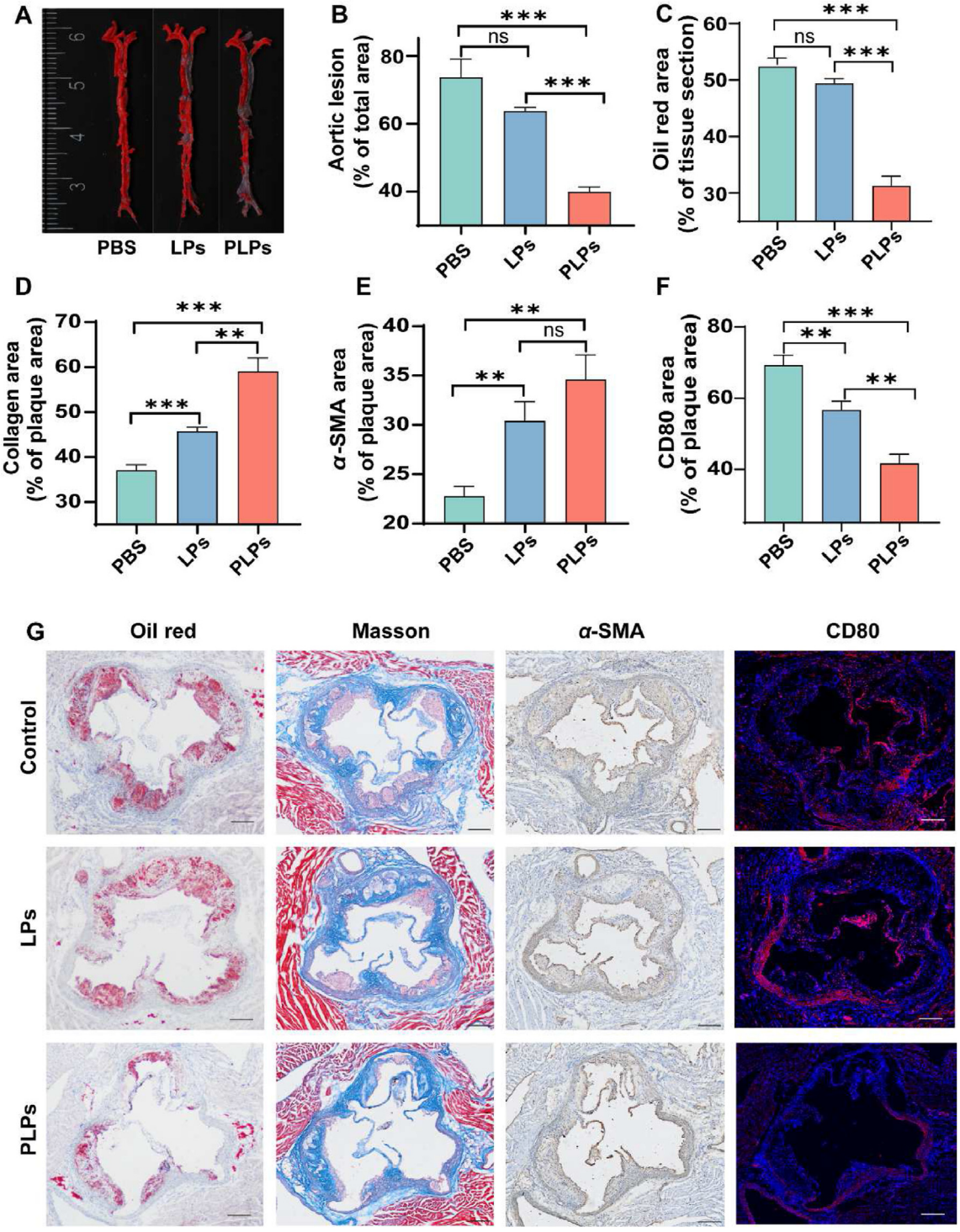

Figure 5 PLPs inhibited atherosclerosis progression *in vivo*. (A) Representative images of oil red O (ORO)-stained atherosclerotic lesions of the aorta en-face and (B) the corresponding quantitative analysis of plaque areas in the total intima area of the aorta. (C−F) Semiquantitative analysis and (G) representative images of aorta root sections stained by ORO (C), Masson's trichrome (D), anti-α-SMA antibodies (E), and anti-CD80 antibodies (F), respectively ($n = 5$ or 6). The atherosclerosis (AS) mouse models were developed by means of feeding $ApoE^{-/-}$ mice with Western Diets *ad libitum*. The AS mice were i.v. administered with PBS, LPs, and PLPs at a dose of 0.5 mg of liposomes every 3 days for 16 weeks. Scale bar = 200 μm. All data were presented as the mean ± SEM. $^{**}P < 0.01$, and $^{***}P < 0.001$. ns, no significant difference.

might be because PLPs could sponge LPS and reverse the expression of the SR-B1 by macrophages. However, the exact mechanisms need to be further elucidated.

Compelling evidence was accumulated to show that risk factors such as diabetes, aging, and obesity would exacerbate gastrointestinal mucosa leakage. Therefore, LPS could be

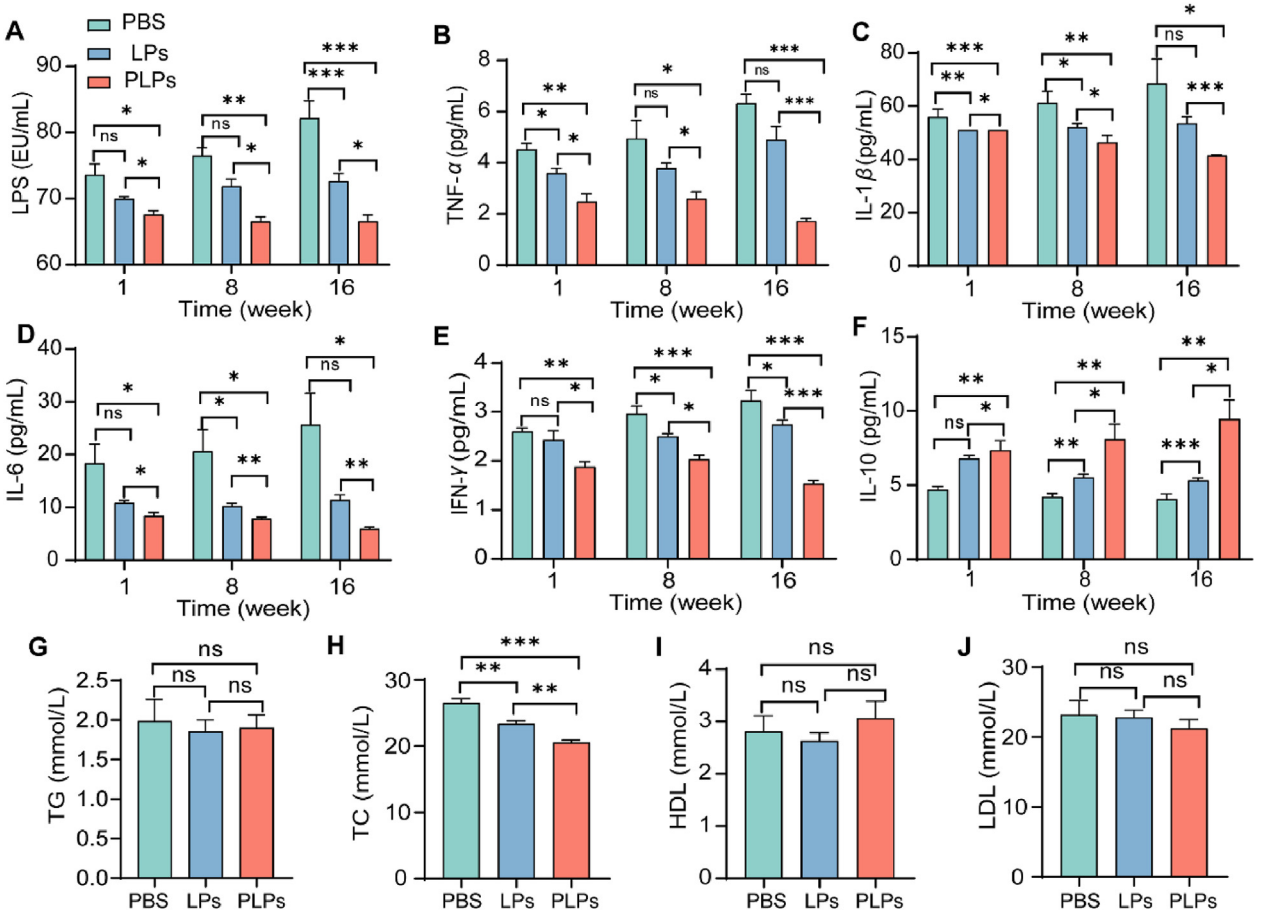

Figure 6 PLPs ameliorated the systematic inflammation response in atherosclerosis (AS) mouse models. (A−F) The serum levels of LPS (A), the inflammatory cytokines including TNF-α (B), IL-1β (C), IL-6 (D), and IFN-γ (E) and IL-10 (F) on the 1st, 8th, and 16th weeks from AS mouse models after different treatments ($n = 4$). (G−J) The serum levels of TG (G), TC (H), HDL (I), and LDL (J) from AS models treated with PBS, LPs, and PLPs at the study endpoint ($n = 5$). All data were presented as the mean ± SEM. $^*P < 0.05$, $^{**}P < 0.01$, and $^{***}P < 0.001$. ns, no significant difference.

released into the circulation, causing systematic chronic inflammation and promoting the development of atherosclerosis[17]. The released LPS mainly derived from gut microbiota, and the proliferation of pathogenic flora and their intimate attachments to gastrointestinal epithelium would be conducive to releasing LPS into circulation[62]. The relationship between gut microbiota and AS development is attracting extensive attention nowadays. It was reported that gavage with live *Bacteroides vulgatus* and *B. dorei* could inhibit bacterial growth and reduce fecal and serum LPS concentration, effectively preventing AS from occurring[63]. This led us to think of the oral formulation of PLPs, which could reduce the level of LPS from the fountainhead and be more convenient for patients. It might be a promising research direction for future study. In addition, IL-23-IL-22 signaling, which could restrain proatherogenic factors such as LPS biosynthesis and destruction of the intestinal barrier, might also function well as the metabolic therapeutic target for AS treatment[64]. Furthermore, apart from AS, LPS was reported to be increased in patients with chronic inflammation states such as obesity and type 2 diabetes[65], and also in acute inflammatory conditions such as sepsis and acute lung injury[66,67]. The PLPs developed in the present study might also be utilized to treat those diseases.

Conventional drugs for AS mainly include anti-hypertension or cholesterol-lowering drugs, such as statins[68]. However, the mechanisms of action of these drugs and PLPs are totally different. While statin drugs primarily focus on inhibiting intracellular cholesterol synthesis from a metabolic blocking perspective, the PLPs in our study aim to remove LPS from the circulation from an inflammation suppression perspective. Therefore, our study did not include conventional drugs as a control group. There is also some cutting-edge research focused on immunotherapies for AS, such as cytokine-orientated therapy or drug delivery systems targeting immune cells to suppress the immune responses caused by inflammation[69]. However, in our study, it might be an alternative strategy to address etiological factors leading to inflammation, such as LPS, that may fundamentally inhibit AS initiation and development.

3.6. *Mechanisms of LPS removal by PLPs in vivo*

To understand the mechanism underlying the fact that PLPs absorbing LPS exerted an inhibitory influence on AS progression, healthy C57/BL6J mice were i.v. administered three kinds of prepared nanomedicines to explore the pharmacokinetic profiles and biodistribution pattern of PLPs. LPS mixed with DiD-labeled

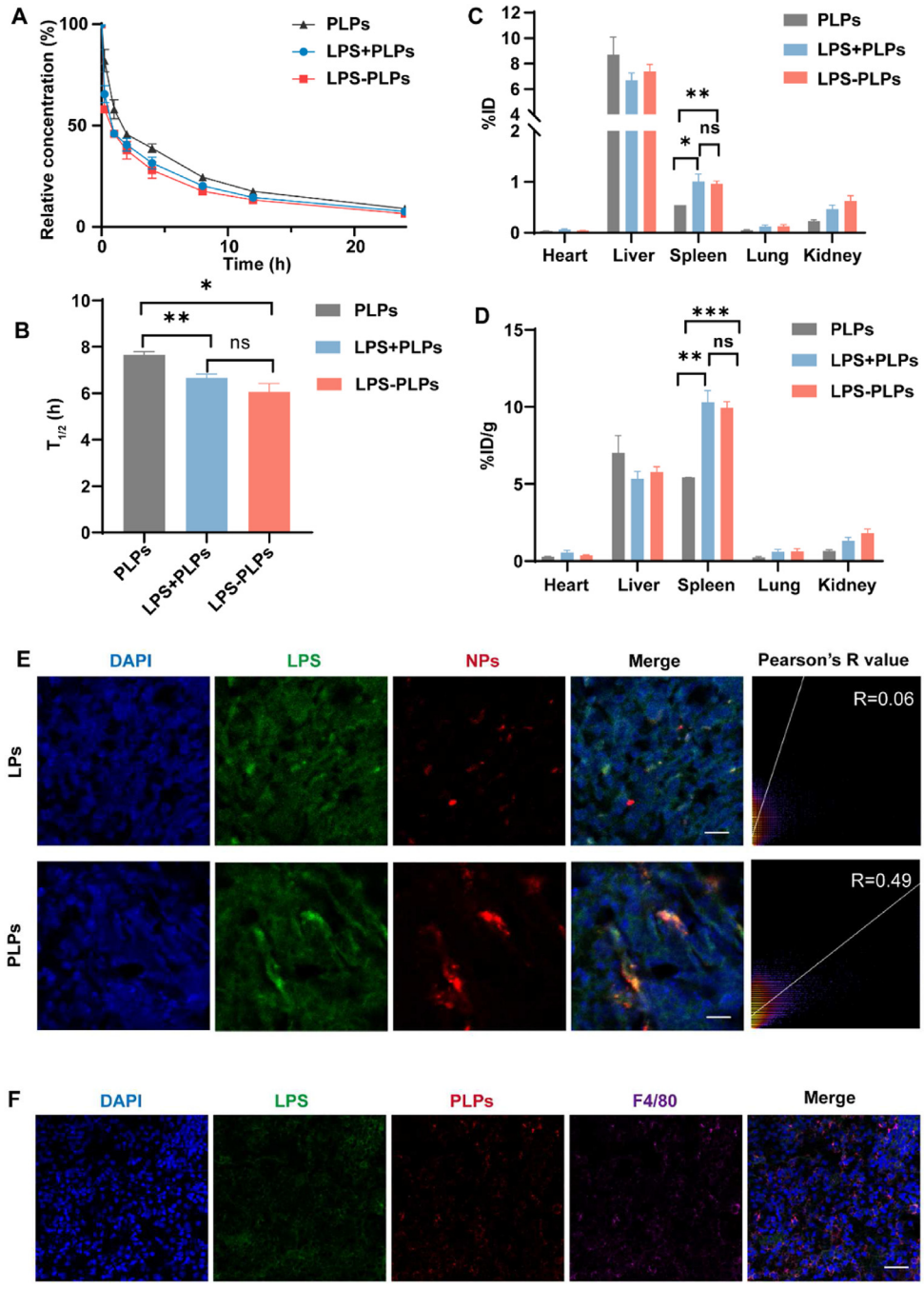

Figure 7 Mechanisms of LPS removal by PLPs *in vivo*. (A) Systemic circulation lifetime of DiD-labeled PLPs *in vivo* by measuring fluorescence signals of DiD in blood samples at various time points. (B) The half-life of DiD-labeled PLPs in circulation. (C, D) Biodistribution of DiD-labeled PLPs at 24 h after i.v. injection. Displayed is the percentage of injected DiD dose (%ID) for each organ (C) and the %ID per gram of tissue (%ID/g) for each organ (D). (E) *In vivo* distribution and colocalization of DiD-labeled liposomes and FITC-LPS in the mouse spleen observed under microscopy and the corresponding Pearson's R value in the LPs and PLPs groups. Scale bar = 20 μm. (F) Representative fluorescence images of the colocalization of LPS, PLPs, and macrophages in spleen sections. Green, FITC-labeled LPS. Red, DiD-labeled LPs or PLPs. Blue, DAPI-stained nucleus. Yellow, green merged with red. Purple, PE-labeled anti-F4/80 antibody. Scale bar = 50 μm. Data were presented as the mean ± SEM ($n = 4$), $^{*}P < 0.05$, $^{**}P < 0.01$, and $^{***}P < 0.001$. ns, no significant difference.

PLPs followed by immediate injection into mice or LPS incubated with DiD-labeled PLPs for 30 min prior to injection were indicated as LPS + PLPs or LPS−PLPs group, respectively. Compared to the PLPs group, both LPS + PLPs and LPS−PLPs groups displayed a rapid decline in the PLPs concentration in the circulation and a shorter elimination half-life (Fig. 7A and B), demonstrating that LPS could sponge PLPs rapidly in the circulation, which rendered them more amenable to be removed from the blood. The major organs of mice were extracted 24 h post-injection to further explore the site where they were eliminated.

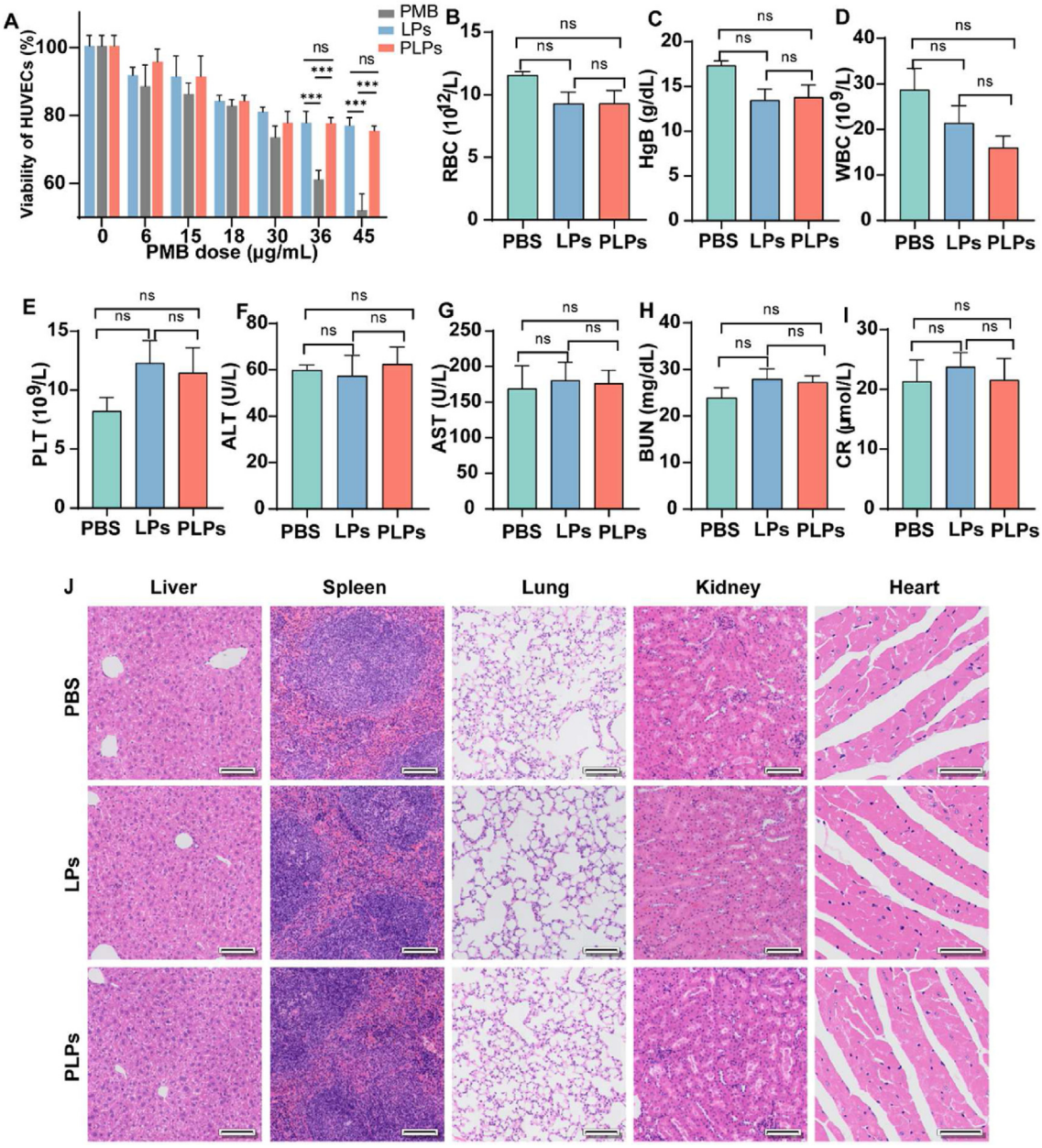

Figure 8 Biocompatibility of PLPs. (A) Viability of HUVECs treated with PMB, LPs, and PLPs with a series of concentrations of PMB (0, 6, 15, 18, 30, 36, and 45 μg/mL) ($n = 4$). (B−I) Blood routine test with indicators including RBC (B), HgB (C), WBC (D), and PLT (E) and hepatorenal function test with indicators including ALT (F), AST (G), BUN (H), and CR (I) was used to assess the biosafety of PLPs. (J) Representative images of major organs (heart, liver, spleen, lung, and kidney) by H&E staining at the study endpoint after different treatments (scale bar = 100 μm). Data were presented as the mean ± SEM ($n = 3$). ***$P < 0.001$. ns, no significant difference.

The histograms showed that similar intensity of DiD fluorescence signals in the spleens was found in both LPS + PLPs and LPS-PLPs groups, which was much stronger than that of the PLPs group (Fig. 7C and D), revealing that rapid and efficient binding to LPS made it easier for PLPs to accumulate in the spleens. Next, the distribution of FITC-LPS and DiD-labeled PLPs in the spleen 8 h post-injection was further explored. The acquired images by CLSM showed that PLPs colocalized much better with LPS compared to LPs, with a larger Pearson's R-value (above threshold) of 0.49 than that of the latter (0.06) (Fig. 7E). The cross-section analysis of the spleen also showed that the red curve overlapped more with the green curve in the PLPs group than that in the LPs group (Supporting Information Fig. S6). These results demonstrated that PLPs could effectively arrest LPS *in vivo*. Furthermore, a much stronger fluorescence intensity of FITC was found in the spleen of PLPs group than that of the LPs group (Supporting Information Fig. S7), indicating more LPS was transported to the spleen in the PLPs group.

The eventual fate of LPS−PLPs complexes *in vivo* was investigated step by step. First, the *in vivo* organ-level distribution (Fig. 7C and D) indicated that the livers and spleens, the primary organs of the mononuclear phagocyte system (MPS), took up

more LPS−PLPs complexes than other organs. Second, the study proceeded to investigate the sub-organ biodistribution of LPS−PLPs in the livers (Supporting Information Fig. S8), and spleens (Fig. 7F). LPS−PLPs complexes were highly colocalized with macrophages marked with F4/80 antibodies in the spleens and livers, consistent with the mechanism study *in vitro* (Fig. 4A), demonstrating that macrophages in the spleens and livers played a dominant role in PLPs-mediated LPS elimination. As PLPs inhibited the systematic inflammation response, it was believed that macrophages in the spleens and livers phagocytosed LPS as the form of LPS−PLPs complexes instead of being activated toward the M1 phenotype through TLR4 activation by LPS. Third, the subcellular localization of LPS−PLPs complexes in macrophages was further explored. The results (Supporting Information Fig. S9) indicated an increasing number of LPS−PLPs were accumulated in BMDMs as time prolonged, and LPS−PLPs always colocalized well with lysosomes (Supporting Information Fig. S9A). Consistently, the cross-section analysis (Supporting Information Figs. S9B-S9D) also showed that both FITC-LPS and DiD-PLPs were highly overlaid with lysosomes, indicating LPS−PLPs complexes were digested in lysosomes after endocytosis by macrophages in livers and spleens. Altogether, compared with LPs, PLPs could bind to LPS more efficiently *in vivo* and render LPS more amenable to be removed from circulation and resolved by lysosomes in macrophages through endocytosis, therefore preventing LPS from activating monocytes in the blood and macrophages in the spleens and livers, diminishing inflammatory responses and eventually inhibiting the progression of AS plaques.

3.7. *Biocompatibility of PLPs*

The cytotoxicity of PLPs was preliminarily evaluated by incubating HUVECs with a series of concentrations of PLPs for 24 h, with LPs and free PMB as control groups. As shown in Fig. 8A, free PMB exhibited high toxicity in a dose-dependent manner, and the toxicity was significantly reduced in both PLPs and LPs groups. The results indicated that PMB loaded by liposomes substantially reduced its toxicity *in vitro* compared with free PMB. Furthermore, to verify whether PLPs could cause a side effect *in vivo*, at the study endpoint of the pharmacodynamics experiment, blood samples and major organs from different treatment groups were collected. Hematology analysis showed no statistically significant differences among the PBS, LPs, and PLPs groups regarding RBC, HgB, WBC, and PLT counts (Fig. 8B−E). In addition, the levels of biochemical indicators, including ALT, AST, BUN, and CR, in the PLPs group were equivalent to those in the PBS and LPs groups (Fig. 8F−I). There were no noticeable pathological changes in mice treated with PLPs compared to the PBS and LPs groups by histologic analysis (Fig. 8J). The weight of the liver, spleen, and body weight at the study endpoint of the pharmacodynamics experiment also exhibited no significant differences among the three groups (Supporting Information Figs. S10A−C). All the results above demonstrated that PLPs harbored a satisfactory safety profile and biocompatibility both *in vitro* and *in vivo*.

4. Conclusions

The fact that LPS could promote AS progression has aroused extensive attention nowadays. In the present study, liposomes with PMB covalently conjugated to the surface (PLPs) were constructed simply and yielded a powerful ability to sponge LPS in a dose-dependent manner. PLPs could inhibit LPS-induced macrophage activation and pro-inflammatory cytokine release, block foam cell formation, stabilize atherosclerotic plaque, and prevent AS progression. The strategy presented by this study also paves the road for managing other LPS-related diseases, including infectious diseases like acute lung injury, sepsis, and metabolic diseases like obesity and type 2 diabetes.

Acknowledgments

The work was supported by the National Natural Science Foundation of China (82070228, 81773283) and the National Key R&D Program of China (No. 2019YFC1316204).

Author contributions

Huiwen Liu carried out experiments and analyzed the data. Honglan Wang wrote the original paper. Qiyu Li provided advice on the creation of animal models. Yiwei Wang provided some material support. Ying He, Xuejing Li, Onder Ergonul, and Füsun Can participated in part of the experiments. Chunyan Sun gave expert advice on compound modification on liposomes. Zhiqing Pang supervised all studies. Bo Zhang revised the manuscript. And Yu Hu conceived the project. All authors have read and approved the final manuscript.

Conflicts of interest

The authors declare no conflicts of interest.

Appendix A. Supporting information

Supporting data to this article can be found online at https://doi.org/10.1016/j.apsb.2023.06.005.

References

1. Shapouri-Moghaddam A, et al. Macrophage plasticity, polarization, and function in health and disease. *J Cell Physiol* 2018;**233**:6425−40.
2. Gencer S, et al. Endothelial ACKR3 drives atherosclerosis by promoting immune cell adhesion to vascular endothelium. *Basic Res Cardiol* 2022;**117**:30.
3. Ridker PM, et al. Anti-inflammatory therapy with canakinumab for atherosclerotic disease. *N Engl J Med* 2017;**377**:1119−31.
4. Moore KJ, Sheedy FJ, Fisher EA. Macrophages in atherosclerosis: a dynamic balance. *Nat Rev Immunol* 2013;**13**:709−21.
5. Li B, Xia Y, Hu B. Infection and atherosclerosis: TLR-dependent pathways. *Cell Mol Life Sci* 2020;**77**:2751−69.
6. Violi F, Cammisotto V, Bartimoccia S, Pignatelli P, Carnevale R, Nocella C. Gut-derived low-grade endotoxaemia, atherothrombosis and cardiovascular disease. *Nat Rev Cardiol* 2023;**20**:24−37.
7. Maldonado RF, Sá-Correia I, Valvano MA. Lipopolysaccharide modification in Gram-negative bacteria during chronic infection. *FEMS Microbiol Rev* 2016;**40**:480−93.
8. Simonsen JR, Järvinen A, Harjutsalo V, Forsblom C, Groop PH, Lehto M. The association between bacterial infections and the risk of coronary heart disease in type 1 diabetes. *J Intern Med* 2020;**288**:711−24.
9. Wiedermann CJ, et al. Association of endotoxemia with carotid atherosclerosis and cardiovascular disease. *J Am Coll Cardiol* 1999;**34**:1975−81.

10. Asada M, et al. Serum Lipopolysaccharide-binding protein levels and the incidence of cardiovascular disease in a general Japanese population: the hisayama study. *J Am Heart Assoc* 2019;**8**:e013628.
11. Zhou X, et al. Gut-dependent microbial translocation induces inflammation and cardiovascular events after ST-elevation myocardial infarction. *Microbiome* 2018;**6**:66.
12. Carnevale R, et al. Low-grade endotoxaemia enhances artery thrombus growth *via* Toll-like receptor 4: implication for myocardial infarction. *Eur Heart J* 2020;**41**:3156−65.
13. Pastori D, et al. Gut-Derived serum lipopolysaccharide is associated with enhanced risk of major adverse cardiovascular events in atrial fibrillation: effect of adherence to mediterranean diet. *J Am Heart Assoc* 2017;**6**:e005784.
14. Carnevale R, et al. Localization of lipopolysaccharide from *Escherichia Coli* into human atherosclerotic plaque. *Sci Rep* 2018;**8**:3598.
15. Chinetti-Gbaguidi G, Colin S, Staels B. Macrophage subsets in atherosclerosis. *Nat Rev Cardiol* 2015;**12**:10−7.
16. Ciesielska A, Matyjek M, Kwiatkowska K. TLR4 and CD14 trafficking and its influence on LPS-induced pro-inflammatory signaling. *Cell Mol Life Sci* 2021;**78**:1233−61.
17. Geng S, et al. The persistence of low-grade inflammatory monocytes contributes to aggravated atherosclerosis. *Nat Commun* 2016;**7**:13436.
18. Bäck M, Ketelhuth DF, Agewall S. Matrix metalloproteinases in atherothrombosis. *Prog Cardiovasc Dis* 2010;**52**:410−28.
19. Derkx B, Wittes J, McCloskey R. Randomized, placebo-controlled trial of HA-1A, a human monoclonal antibody to endotoxin, in children with meningococcal septic shock. European pediatric meningococcal septic shock trial study group. *Clin Infect Dis* 1999;**28**:770−7.
20. Kellum JA, Formeck CL, Kernan KF, Gomez H, Carcillo JA. Subtypes and mimics of sepsis. *Crit Care Clin* 2022;**38**:195−211.
21. Jiang L, et al. Endotoxin-adsorbing macrophage-mimetic hybrid liposome for sepsis treatment. *Chem Eng J* 2019;**371**:15−25.
22. Seager Danciger J, et al. Method for large scale isolation, culture and cryopreservation of human monocytes suitable for chemotaxis, cellular adhesion assays, macrophage and dendritic cell differentiation. *J Immunol Methods* 2004;**288**:123−34.
23. Nang SC, et al. Polymyxin causes cell envelope remodelling and stress responses in mcr-1-harbouring. *Escherichia coli. Int J Antimicrob Agents* 2022;**59**:106505.
24. Tsubery H, Ofek I, Cohen S, Fridkin M. The functional association of polymyxin B with bacterial lipopolysaccharide is stereospecific: studies on polymyxin B nonapeptide. *Biochemistry* 2000;**39**:11837−44.
25. Srimal S, Surolia N, Balasubramanian S, Surolia A. Titration calorimetric studies to elucidate the specificity of the interactions of polymyxin B with lipopolysaccharides and lipid A. *Biochem J* 1996;**315**:679−86.
26. Ziv G, Nouws JF, van Ginneken CA. The pharmacokinetics and tissue levels of polymyxin B, colistin and gentamicin in calves. *J Vet Pharmacol Therapeut* 1982;**5**:45−58.
27. Falagas ME, Kasiakou SK. Toxicity of polymyxins: a systematic review of the evidence from old and recent studies. *Crit Care* 2006;**10**:R27.
28. Allen TM, Cullis PR. Liposomal drug delivery systems: from concept to clinical applications. *Adv Drug Deliv Rev* 2013;**65**:36−48.
29. Papahadjopoulos D, et al. Sterically stabilized liposomes: improvements in pharmacokinetics and antitumor therapeutic efficacy. *Proc Natl Acad Sci U S A* 1991;**88**:11460−4.
30. Jiang L, et al. Bacteria-anchoring hybrid liposome capable of absorbing multiple toxins for antivirulence therapy of escherichia coli infection. *ACS Nano* 2021;**15**:4173−85.
31. Chiang SCC, et al. Quercetin ameliorates XIAP deficiency associated hyperinflammation. *Blood* 2022;**140**:706−15.
32. Keyel PA, Tkacheva OA, Larregina AT, Salter RD. Coordinate stimulation of macrophages by microparticles and TLR ligands induces foam cell formation. *J Immunol* 2012;**189**:4621−9.
33. Wu Y, et al. An apoptotic body-biomimic liposome in situ upregulates anti-inflammatory macrophages for stabilization of atherosclerotic plaques. *J Control Release* 2019;**316**:236−49.
34. Zhang B, et al. Fibrin degradation by rtPA enhances the delivery of nanotherapeutics to A549 tumors in nude mice. *Biomaterials* 2016;**96**:63−71.
35. Zhang B, et al. LDLR-mediated peptide-22-conjugated nanoparticles for dual-targeting therapy of brain glioma. *Biomaterials* 2013;**34**:9171−82.
36. Benn G, et al. Phase separation in the outer membrane of Escherichia coli. *Proc Natl Acad Sci U S A* 2021;**118**:e2112237118.
37. Lithgow T, Stubenrauch CJ, Stumpf MPH. Surveying membrane landscapes: a new look at the bacterial cell surface. *Nat Rev Microbiol* 2023;**21**:502−18.
38. Lee S, Bayley H. Reconstruction of the gram-negative bacterial outer-membrane bilayer. *Small* 2022;**18**:e2200007.
39. Wang Y, Jia Q, Zhang Y, Wei J, Liu P. Amygdalin attenuates atherosclerosis and plays an anti-inflammatory role in *ApoE* knock-out mice and bone marrow-derived macrophages. *Front Pharmacol* 2020;**11**:590929.
40. Zhang BC, Li Z, Xu W, Xiang CH, Ma YF. Luteolin alleviates NLRP3 inflammasome activation and directs macrophage polarization in lipopolysaccharide-stimulated RAW264.7 cells. *Am J Transl Res* 2018;**10**:265−73.
41. Du M, et al. Absence of interferon regulatory factor 1 protects against atherosclerosis in apolipoprotein E-deficient mice. *Theranostics* 2019;**9**:4688−703.
42. Yao Z, et al. Blood-borne lipopolysaccharide is rapidly eliminated by liver sinusoidal endothelial cells *via* high-density lipoprotein. *J Immunol* 2016;**197**:2390−9.
43. Zheng Y, et al. Mettl14 mediates the inflammatory response of macrophages in atherosclerosis through the NF-*k*B/IL-6 signaling pathway. *Cell Mol Life Sci* 2022;**79**:311.
44. Wiesner P, et al. Low doses of lipopolysaccharide and minimally oxidized low-density lipoprotein cooperatively activate macrophages *via* nuclear factor *κ*B and activator protein-1: possible mechanism for acceleration of atherosclerosis by subclinical endotoxemia. *Circ Res* 2010;**107**:56−65.
45. Yuan Q, Tang B, Zhang C. Signaling pathways of chronic kidney diseases, implications for therapeutics. *Signal Transduct Targeted Ther* 2022;**7**:182.
46. Evans CJ, Liu T, Girard JR, Banerjee U. Injury-induced inflammatory signaling and hematopoiesis in. *Drosophila. Proc Natl Acad Sci U S A* 2022;**119**:e2119109119.
47. Xu M, et al. Osteopontin targeted theranostic nanoprobes for laser-induced synergistic regression of vulnerable atherosclerotic plaques. *Acta Pharm Sin B* 2022;**12**:2014−28.
48. Song Y, et al. Platelet membrane-coated nanoparticle-mediated targeting delivery of rapamycin blocks atherosclerotic plaque development and stabilizes plaque in apolipoprotein E-deficient ($ApoE^{-/-}$) mice. *Nanomedicine* 2019;**15**:13−24.
49. Gao C, et al. Treatment of atherosclerosis by macrophage-biomimetic nanoparticles *via* targeted pharmacotherapy and sequestration of proinflammatory cytokines. *Nat Commun* 2020;**11**:2622.
50. Li X, et al. Liposomal codelivery of inflammation inhibitor and collagen protector to the plaque for effective anti-atherosclerosis. *Chin Chem Lett* 2023;**34**:107483.
51. Muckian C, Fitzgerald A, O'Neill A, O'Byrne A, Fitzgerald DJ, Shields DC. Genetic variability in the extracellular matrix as a determinant of cardiovascular risk: association of type III collagen COL3A1 polymorphisms with coronary artery disease. *Blood* 2002;**100**:1220−3.
52. Fanaroff AC, et al. Frequency, regional variation, and predictors of undetermined cause of death in cardiometabolic clinical trials: a pooled analysis of 9259 deaths in 9 trials. *Circulation* 2019;**139**:863−73.

53. Chistiakov DA, Bobryshev YV, Nikiforov NG, Elizova NV, Sobenin IA, Orekhov AN. Macrophage phenotypic plasticity in atherosclerosis: the associated features and the peculiarities of the expression of inflammatory genes. *Int J Cardiol* 2015;**184**:436−45.
54. Saito Y, et al. Structural differences in bacterial lipopolysaccharides determine atherosclerotic plaque progression by regulating the accumulation of neutrophils. *Atherosclerosis* 2022;**358**:1−11.
55. Shan Y, et al. Protective effect of sulforaphane on human vascular endothelial cells against lipopolysaccharide-induced inflammatory damage. *Cardiovasc Toxicol* 2010;**10**:139−45.
56. Luo P, et al. Celastrol mitigates inflammation in sepsis by inhibiting the PKM2-dependent Warburg effect. *Mil Med Res* 2022;**9**:22.
57. Baidzajevas K, et al. Macrophage polarisation associated with atherosclerosis differentially affects their capacity to handle lipids. *Atherosclerosis* 2020;**305**:10−8.
58. Castoldi A, et al. Triacylglycerol synthesis enhances macrophage inflammatory function. *Nat Commun* 2020;**11**:4107.
59. Panousis CG, Zuckerman SH. Interferon-gamma induces down-regulation of Tangier disease gene (ATP-binding-cassette transporter 1) in macrophage-derived foam cells. *Arterioscler Thromb Vasc Biol* 2000;**20**:1565−71.
60. Taront S, et al. Implication of scavenger receptors in the interactions between diesel exhaust particles and immature or mature dendritic cells. *Part Fibre Toxicol* 2009;**6**:9.
61. Baranova I, et al. Lipopolysaccharide down regulates both scavenger receptor B1 and ATP binding cassette transporter A1 in RAW cells. *Infect Immun* 2002;**70**:2995−3003.
62. Emoto T, et al. Analysis of gut microbiota in coronary artery disease patients: a possible link between gut microbiota and coronary artery disease. *J Atherosclerosis Thromb* 2016;**23**:908−21.
63. Yoshida N, et al. Bacteroides vulgatus and bacteroides dorei reduce gut microbial lipopolysaccharide production and inhibit atherosclerosis. *Circulation* 2018;**138**:2486−98.
64. Fatkhullina AR, et al. An interleukin-23-interleukin-22 axis regulates intestinal microbial homeostasis to protect from diet-induced atherosclerosis. *Immunity* 2018;**49**:943. 57.e9.
65. Creely SJ, et al. Lipopolysaccharide activates an innate immune system response in human adipose tissue in obesity and type 2 diabetes. *Am J Physiol Endocrinol Metab* 2007;**292**:E740−7.
66. Anderson ST, Commins S, Moynagh PN, Coogan AN. Lipopolysaccharide-induced sepsis induces long-lasting affective changes in the mouse. *Brain Behav Immun* 2015;**43**:98−109.
67. Chen H, Bai C, Wang X. The value of the lipopolysaccharide-induced acute lung injury model in respiratory medicine. *Expet Rev Respir Med* 2010;**4**:773−83.
68. Kim M, et al. Targeted delivery of anti-inflammatory cytokine by nanocarrier reduces atherosclerosis in *ApoE*$^{-/-}$ mice. *Biomaterials* 2020;**226**:119550.
69. Xiao Q, et al. Biological drug and drug delivery-mediated immunotherapy. *Acta Pharm Sin B* 2021;**11**:941−60.